Science and Technology Indonesia
e-ISSN:2580-4391 *p*-ISSN:2580-4405
Vol. 11, No. 2, April 2026

Research Paper

Hierarchically Structured Zn-Al LDH/Hydrochar from Rambutan Peel (*Nephelium lappaceum* L.) for Enhanced Fe(II) Adsorption

Desti Erviana[1,2], Normah Normah[2,3], Heroldinho Arieveali[1,2], Navinda Ramadhan[1,2*]

[1]*Master Program of Materials Science, Graduate School, Universitas Sriwijaya, South Sumatra, Palembang, 30139, Indonesia*
[2]*Research Center of Inorganic Materials and Coordination Complexes, Universitas Sriwijaya, South Sumatra, Palembang, 30139, Indonesia*
[3]*Departement of Chemistry, Universitas Indo Global Mandiri, South Sumatra, Palembang, 30129, Indonesia*
***Corresponding author**: navindaramadhanofficial@gmail.com

Abstract
Dissolved ferrous ions in water pose significant environmental and operational challenges, necessitating efficient and sustainable removal technologies. In this study, a hybrid adsorbent was developed by integrating Zn-Al layered double hydroxide (LDH) with hydrochar derived from rambutan peel (*Nephelium lappaceum* L.) via coprecipitation. Characterization confirmed successful composite formation with a substantial increase in specific surface area from 9.621 $m^2.g^{-1}$ for pristine Zn-Al LDH to 52.964 $m^2.g^{-1}$ for the composite, accompanied by enlarged pore volume and enriched oxygen-containing functional groups. Batch adsorption experiments showed strong pH dependence, with optimal Fe(II) removal at pH 6 and equilibrium reached within 120 min. The Zn-Al LDH@NL-HC composite exhibited a markedly higher adsorption capacity (51.501 $mg.g^{-1}$) compared with Zn-Al LDH (15.692 $mg.g^{-1}$) and hydrochar alone (8.594 $mg.g^{-1}$), indicating a significant synergistic effect. Isotherm analysis revealed a maximum adsorption capacity of 76.336 $mg.g^{-1}$ at elevated temperature, while kinetic data followed a pseudo-second-order model, suggesting chemisorption-dominated uptake. Thermodynamic parameters indicated an endothermic and spontaneous process. Regeneration studies demonstrated excellent stability, with adsorption efficiency maintained at 79.48% after five cycles. The superior performance is attributed to combined mechanisms including electrostatic attraction, surface complexation with oxygen-rich groups, ion exchange within LDH interlayers, and diffusion into mesoporous structures. These findings demonstrate the effective valorization of agricultural waste into a high-performance and reusable adsorbent for Fe(II) remediation in aqueous systems.

Keywords
Layered Double Hydroxide, Biomass-Derived Hydrochar, Fe(II) Adsorption, Heavy Metal Removal, Sustainable Adsorbent

Received: 16 December 2025, Accepted: 18 February 2026
https://doi.org/10.26554/sti.2026.11.2.524-537

1. INTRODUCTION

The contamination of aquatic environments by dissolved heavy metals remains a persistent global challenge due to their non-biodegradable nature, toxicity, and long-term ecological impacts. Unlike organic pollutants, heavy metals cannot be mineralized and therefore tend to accumulate in water bodies and sediments, posing chronic risks to ecosystems and human health (Singh et al., 2024). Among various metal ions, ferrous iron (Fe(II)) is frequently detected in groundwater and industrial effluents, particularly from mining, steel processing, and electroplating activities (Xiao et al., 2024). Although iron is an essential micronutrient, excessive Fe(II) concentrations can significantly deteriorate water quality, accelerate pipeline corrosion, induce discoloration and turbidity, and disrupt aquatic habitats (Yao et al., 2025). Furthermore, the oxidation of Fe(II) to Fe(III) often results in uncontrolled precipitation and sludge formation, complicating downstream treatment processes. These challenges underscore the necessity for efficient, selective, and operationally simple technologies for Fe(II) removal.

Conventional iron removal strategies, including chemical oxidation, membrane filtration, ion exchange, and biological treatment, have been widely implemented (Shafie et al., 2025). However, these approaches frequently suffer from high chemical consumption, membrane fouling, sludge generation, or elevated operational costs, limiting their sustainability and scalability (Fitri and Ardiansyah, 2023; Wijaya et al., 2021). In this context, adsorption has emerged as a promising alternative owing to its simplicity, flexibility, and compatibility with decentralized water treatment systems (Meftah et al., 2025; Shabbirahmed et al., 2025). Nevertheless, the overall effectiveness of adsorption is strongly governed by the physicochemical properties of the adsorbent, particularly the accessibility of

active sites, structural stability, and resistance to aggregation (Khan et al., 2025; Kudaibergenova et al., 2026; Tee et al., 2022).

Layered double hydroxides (LDHs) have attracted considerable interest as multifunctional adsorbents due to their tunable metal composition, high surface reactivity, and unique lamellar architecture (Hadnadjev-Kostic et al., 2025; Asri et al., 2020). ZnAl-LDH, in particular, exhibits favorable chemical stability and strong affinity toward metal ions through surface complexation and electrostatic interactions (Normah et al., 2021). Despite these advantages, pristine LDHs are prone to particle agglomeration and restacking of layers, which reduce accessible active sites and limit adsorption performance (Bai et al., 2024; Gao et al., 2025). In addition, structural instability under repeated adsorption-desorption cycles may compromise long-term applicability (Alcalde-Garcia et al., 2023). These inherent limitations highlight the need for rational structural engineering strategies to improve dispersion, stability, and interfacial reactivity.

Hybridization of LDHs with carbonaceous materials has emerged as an effective strategy to address these limitations (Taher et al., 2023). The incorporation of biomass-derived carbon supports can enhance structural dispersion, introduce additional functional groups, and create synergistic adsorption interfaces (Khosrowshahi et al., 2022; Kundu et al., 2024). Hydrochar obtained from hydrothermal carbonization is particularly attractive because it can be produced from renewable biomass under relatively mild conditions while retaining abundant oxygen-containing functional groups such as –OH and –COOH (Durak et al., 2026). These surface functionalities facilitate metal ion coordination and promote stronger interfacial interaction between the inorganic LDH layers and the carbon matrix (Hao, 2025). However, the performance enhancement of LDH-carbon composites is highly dependent on precursor selection, interfacial compatibility, and structural integration, which remain insufficiently optimized in many reported systems.

Recent studies have demonstrated the potential of LDH-based carbon composites for metal ion removal, including systems incorporating biochar, activated carbon, or graphene-derived materials (Huang et al., 2022; Sikri et al., 2025). These composites generally exhibit improved adsorption efficiency compared to pristine LDHs due to enhanced dispersion and additional binding sites (Juleanti et al., 2021). Nevertheless, many reported materials rely on chemically activated carbons or synthetic carbon nanostructures, which may increase production cost and reduce sustainability (Tyagi and Anand, 2024). Moreover, several biomass-derived carbons show limited structural homogeneity or weak interfacial coupling with LDH layers, resulting in moderate performance gains (El-Sawaf et al., 2025). These observations indicate that the selection of a suitable biomass precursor and a controlled integration strategy are critical to achieving meaningful synergistic effects in LDH-carbon composites.

Agricultural waste represents a promising yet underutilized precursor for functional hydrochar production. *Nephelium lappaceum* L. (rambutan) peel waste is abundantly generated in tropical regions and is rich in lignocellulosic components and reactive surface functionalities, making it an attractive sustainable carbon source (Khir et al., 2025; Torgbo et al., 2024). Converting this biomass into hydrochar not only mitigates solid waste accumulation but also aligns with circular economy principles by transforming agricultural residues into value-added functional materials. Despite this potential, the controlled integration of rambutan-derived hydrochar with ZnAl-LDH for selective Fe(II) adsorption has not been systematically explored, particularly in terms of structural synergy and adsorption stability (Cedeño-Muñoz et al., 2026).

In this study, we report a sustainable ZnAl-LDH/hydrochar composite synthesized via a facile coprecipitation strategy by integrating ZnAl-LDH with hydrochar derived from *Nephelium lappaceum* L. waste. The structural, morphological, thermal, and surface characteristics of the composite were systematically investigated using X-ray diffraction (XRD), Fourier-transform infrared spectroscopy (FTIR), scanning electron microscopy (SEM), thermogravimetric-differential thermal analysis (TG-DTA), and Brunauer-Emmett-Teller (BET) analysis. The developed material demonstrates high selectivity toward Fe(II) and excellent reusability. The improved performance is attributed to the synergistic interaction between the layered inorganic framework and the biomass-derived carbon matrix, which enhances dispersion, suppresses agglomeration, and provides abundant accessible active sites. This work provides a rational and sustainable design approach for LDH-based composites and advances the development of environmentally friendly materials for efficient water purification.

2. EXPERIMENTAL SECTION

2.1 Chemicals and Instrumentals

The chemicals used are Zinc Nitrate Hexahydrate ($Zn(NO_3)_2.6H_2O$), Aluminium Nitrate Nanohydrate ($Al(NO_3)_3.9H_2O$), Sodium Hydroxide (NaOH), Hydrochloric Acid (HCl), Nitric Acid (HNO_3), Iron(II) Chloride Tetrahydrate ($\cdot 4H_2O$), Acetate Buffer Solution (CH_3COONa), 1,10-Phenanthroline ($C_{12}H_8N_2.H_2O$), Hydroxylamine Chloride ($HONH_3Cl$), Distilled Water and Rambutan Peel (*Nephelium lappaceum* L.)

The instruments used were XRD Rigaku Miniflex-6000, FT-IR Shimadzu Prestige-21, Nitrogen Adsorption Desorption Equipment Quantachrome Instruments, Scanning Electron Miscroscope SU800 Series, Image-J software to analyze particle distribution in the material, TG-DTA Shimadzu DTG-60H, UV-Vis Spectrophotometer Biobase BK-UV 1800 PC and Hydrothermal stainless-steel autoclave.

2.2 Synthesis ZnAl LDH

Synthesis of ZnAl LDH was carried out using the Coprecipitation method (Lesbani et al., 2025; Mohadi et al., 2022). 100 mL of 0.75 M $Zn(NO_3)_2.6H_2O$ was mixed with 100 mL of 0.25 M $Al(NO_3)_3.9H_2O$. The mixture was then dripped with 2 M NaOH solution until pH 10 and stirred for 20 hours at

temperature of 80°C. After that, the precipitate was filtered and rinsed with distilled water. The precipitate was dried using oven. The resulting solid was characterized using XRD, FTIR, BET, SEM and TG-DTA instruments.

2.3 Preparation of NL-HC from Rambutan (*Nephelium lappaceum* L.) Peel

A total of 2.5 g of Rambutan (*Nephelium lappaceum* L.) peel powder was added with 50 mL of distilled water and placed in a hydrothermal stainless steel autoclave (Ramadhan et al., 2025). The mixture was then heated at 200°C for 10 hours. The resulting solid, in the form of hydrochar, was filtered and dried until dry. Named with HC-NL. The hydrochar solid was then characterized using XRD, FTIR, BET, SEM, and TG-DTA.

2.4 Preparation of Zn-Al LDH@NL-HC

Zn-Al LDH@NL-HC was prepared using the Coprecipitation method (Badaruddin et al., 2026). A total of 15 mL of 0.75 M $Zn(NO_3)_2.6H_2O$ solution and 15 mL of 0.25 M $Al(NO_3)_3.9H_2O$ solution were mixed and adjusted to pH 10 using NaOH. The mixture was stirred for 1 hour and 3 g of hydrochar was added. The mixture was then set at a temperature of 80°C for 3 days. The precipitate was filtered, dried using an oven and the resulting solid was characterized using XRD, FTIR, BET, SEM and TG-DTA.

2.5 Adsorption-Desorption Study

2.5.1 Effect of pH

20 mL of Fe(II) with a concentration of 10 mg/L was used to study the effect of pH on adsorption. 0.02 g of adsorbent was added to a 100 mL Erlenmeyer flask filled with the sample. The pH of the solution was adjusted to 2-11 using sodium hydroxide (NaOH) and hydrochloric acid (HCl) solutions. The solution was stirred for 2 hours. The separation process was carried out by centrifugation, and the absorbance of the obtained filtrate was measured using a UV-Vis spectrophotometer after complexing with 1,10-phenanthroline. The adsorption capacity was calculated using Equation (1):

$$Q_e = \frac{(C_0 - C_e)V}{m} \tag{1}$$

Where Q_e is the adsorption capacity (mg/g), C_0 is the initial concentration, C_e is the final concentration, m is the mass of the adsorbent (g), and V is the volume of the solution (L).

2.6 Kinetic, Thermodynamic, Isotherm, and Desorption Analysis

The effect of adsorption contact time on the adsorbent can be studied by varying the contact time between the adsorbate and the adsorbent. Adsorption kinetics were calculated using pseudo-first-order and pseudo-second-order equations (Equations (2) and (3)).

$$\log(Q_e - Q_t) = \log Q_e - \left(\frac{k_1}{2.303}\right) t \tag{2}$$

$$\frac{1}{Q_t} = \frac{1}{k_2 Q_e^2} + \frac{1}{Q_e} t \tag{3}$$

Where Q_e is the adsorption capacity at equilibrium (mg/g), Q_t is the adsorption capacity at t (mg/g), t is the adsorption time (minutes), k_1 is the kinetic adsorption rate constant at pseudo-first order (minute^{-1}), and k_2 is the kinetic adsorption rate constant at pseudo-second order (g/mg min).

The isotherm parameters are calculated based on the Langmuir and Freundlich equations (Equations (4) and (5)).

$$\frac{C_e}{Q_e} = \frac{C_e}{Q_m} + \frac{1}{Q_m K_L} \tag{4}$$

$$\log Q_e = \log K_F + 1/n \log C_e \tag{5}$$

Where C_e is the metal ion concentration at equilibrium (mg/L), Q_e is the adsorption capacity at equilibrium (mg/g), Q_m is the maximum adsorption capacity (mg/g), K_L is the Langmuir isotherm equilibrium constant, K_F is the Freundlich isotherm equilibrium constant, and n is the adsorption intensity.

Furthermore, the thermodynamic parameters are analyzed through calculations using Equation (6).

$$\ln \frac{Q_e}{C_e} = \frac{\Delta S}{R} - \frac{\Delta H}{RT} \tag{6}$$

Meanwhile, the Gibbs free energy in the adsorption process is calculated using Equation (7).

$$\Delta G = \Delta H - T\Delta S \tag{7}$$

where R is the Universal Gas Constant, T is Temperature (K), ΔG is Gibbs Free Energy (kJ/mol), ΔH is Enthalpy (kJ/mol), and ΔS is Entropy (J/mol K).

The percentage of desorption is calculated based on the number of Fe(II) metal ions adsorbed through Equation (8).

$$\%D = \frac{C_d}{C_a} \times 100\% \tag{8}$$

where $\%D$ is the percentage of desorbed Fe(II) metal ions, C_a is the number of adsorbed Fe(II) metal ions (mg), and C_d is the number of desorbed Fe(II) metal ions (mg).

2.6. Regeneration Study

The regeneration process was carried out by mixing the desorbed adsorbent with 50 mL of a 100 mg/L Fe(II) metal ion solution. The mixture was stirred for 2 hours, and the residual concentration was measured using a UV-Vis spectrophotometer. The adsorbent was dried and, after drying, used for the desorption process by adding 25 mL of the best desorption reagent and stirring for 2 hours. The filtrate was then complexed with 1,10-phenanthroline and measured using a UV-Vis spectrophotometer. The residue was then dried and reused using a similar procedure for five cycles. The effectiveness of the adsorbent in regeneration can be calculated using Equation (9).

$$\%Regeneration = \frac{Q_r}{Q_0} \times 100\% \quad (9)$$

where Q_0 is the initial Fe(II) metal ion adsorption capacity (mg/g) and Q_r is the Fe(II) metal ion adsorption capacity after regeneration (mg/g).

3. RESULT AND DISCUSSIONS

3.1 Characterization

XRD analysis is implemented to identify crystal structure, material phases, and structural changes before and after composite formation. Zn-Al LDH has typical peaks at 2θ = 10.15°, 19.98°, 32.01°, 33.77°, 39.11°, 58.7°, and 60.02° presented in Figure 1a. These distinctive peaks are oriented to the crystal plane 003, 006, 009, 012, 015, 018, 110 in succession. The layered structure of the LDH is characterized by the creation of a sharp peak at 2θ = 10.15° in accordance with JCPDS No. 48-1023 (Wibiyan et al., 2024). These sharp peaks indicate high crystallinity occupying space in the Zn-Al LDH structure (Wijaya et al., 2025). The NL-HC peak is found at 2θ = 22.20° with an orientation of 002. The presence of hydrochars in Zn-Al LDH provides a change in the crystal orientation of the material. The weakened peaks of 2θ at 32.01° and 33.77° due to the incorporation of NL-HC in the Zn-Al LDH structure create a weak hydrogen bond between the hydrochar and the hydroxyl group (H_2O deformed) in the Zn-Al LDH. In addition, it is also caused by the presence of organic components of NL-HC that cause disturbances in crystal growth. Therefore, peak widening is formed at 2θ = 9.78° and 60.24° which indicates the process of hydrolysis of the hemicellulose and lignin segments of the rambutan peel during hydrothermal carbonization (Kohzadi et al., 2023). The results of this XRD analysis confirm that the layered structure of LDH is maintained and the success of Zn-Al formation of Zn-Al LDH@NL-HC has been successfully verified.

The chemical function groups and interactions between the components that make up the composite material were evaluated using the FTIR instrument on the composite. Figure 1b shows the presence of vibration of the -OH group of the water molecule at 3448 cm^{-1}. The presence of hydroxyl groups in Zn-Al LDH is also confirmed by bending vibrations at 1650 cm^{-1} associated with deformation of adsorbed water molecules (Jefri et al., 2025). The NO_3^- anion occupying the space between LDH layers is characterized by a vibration band at 1371 cm^{-1} (Mohadi et al., 2022). The incorporation of NL-HC in Zn-Al LDH causes a shift in the strain vibration band of the −OH group to 3425 cm^{-1} (Ramadhan et al., 2026). The absorption band at 2967 cm^{-1} is associated with a $-CH_2$ vibration which implies the presence of aliphatic carbon bonds of organic components on the hydrochar surface. In addition, the successful integration of NL-HC into the Zn-Al structure of LDH is characterized by an increase in band intensity at 1600-1500 cm^{-1}. This shows the presence of aromatic C=C, C=O, and −COO (carboxyl) groups derived from hydrochar organic components, such as cellulose and lignin (Nassar et al., 2023). The C−O bond of cellulose from hydrochar was also successfully verified at 1056 cm^{-1}. Meanwhile, bands detected in the wavenumber range from 500 to 800 cm^{-1} imply the presence of metal oxide vibrations in the M−O−M bonds derived from divalent and trivalent metals in LDH structures. Therefore, the formation of Zn-Al LDH@NL-HC was successfully verified along with the results of the difractograms discussed earlier.

The BET characterization method was applied to investigate the properties of surface texture, specifically surface area (S_{BET}) and pore structure that greatly affect the performance of the adsorbent. All synthesized materials imply N_2 type IV adsorption-desorption isotherms and H3 type hysteresis loops, as shown in Figure 1c-e. Type IV adsorption-desorption indicated that the material analyzed had a meso-sized pore structure in the range of 2 to 50 nm (Wibiyan et al., 2024). Meanwhile, the H3 type indicates that the material has non-rigid aggregates, so it is advantageous for the adsorption process. Zn-Al LDH has a surface area of 9.621 $m^2.g^{-1}$. The SBET increased significantly to 52.964 $m^2.g^{-1}$ when Zn-Al LDH was introduced with rambutan bark hydrochar. The increase occurred because NL-HC had an SBET of 52,964 $m^2.g^{-1}$. In addition, there was an increase in pore volume from 0.017 $cm^3.g^{-1}$ in Zn-Al LDH to 0.113 $cm^3.g^{-1}$ in Zn-Al LDH@NL-HC. The findings show that the incorporation of hydrochar in Zn-Al LDH can increase surface area and pore volume which has the potential to have a positive impact on the metal adsorption process. This is linear with previous research (Hamad et al., 2024). A larger S_{BET} and a suitable pore structure can provide more active sites and space to bind to metal ions. In addition, the improvement of the two parameters can promote an effective interface reaction between metal ions and Zn-Al LDH@NL-HC surfaces.

The SEM-EDX instrument was applied to study the surface morphology and composition of its constituent elements microly. Figure 2a-c shows the surface morphology of Zn-Al LDH, NL-HC, and Zn-Al LDH@NL-HC. ZnAl LDH has a morphology with a rough surface in the form of interconnected plates. The findings can be attributed to the results of XRD data that the material has good crystallinity with layered structural

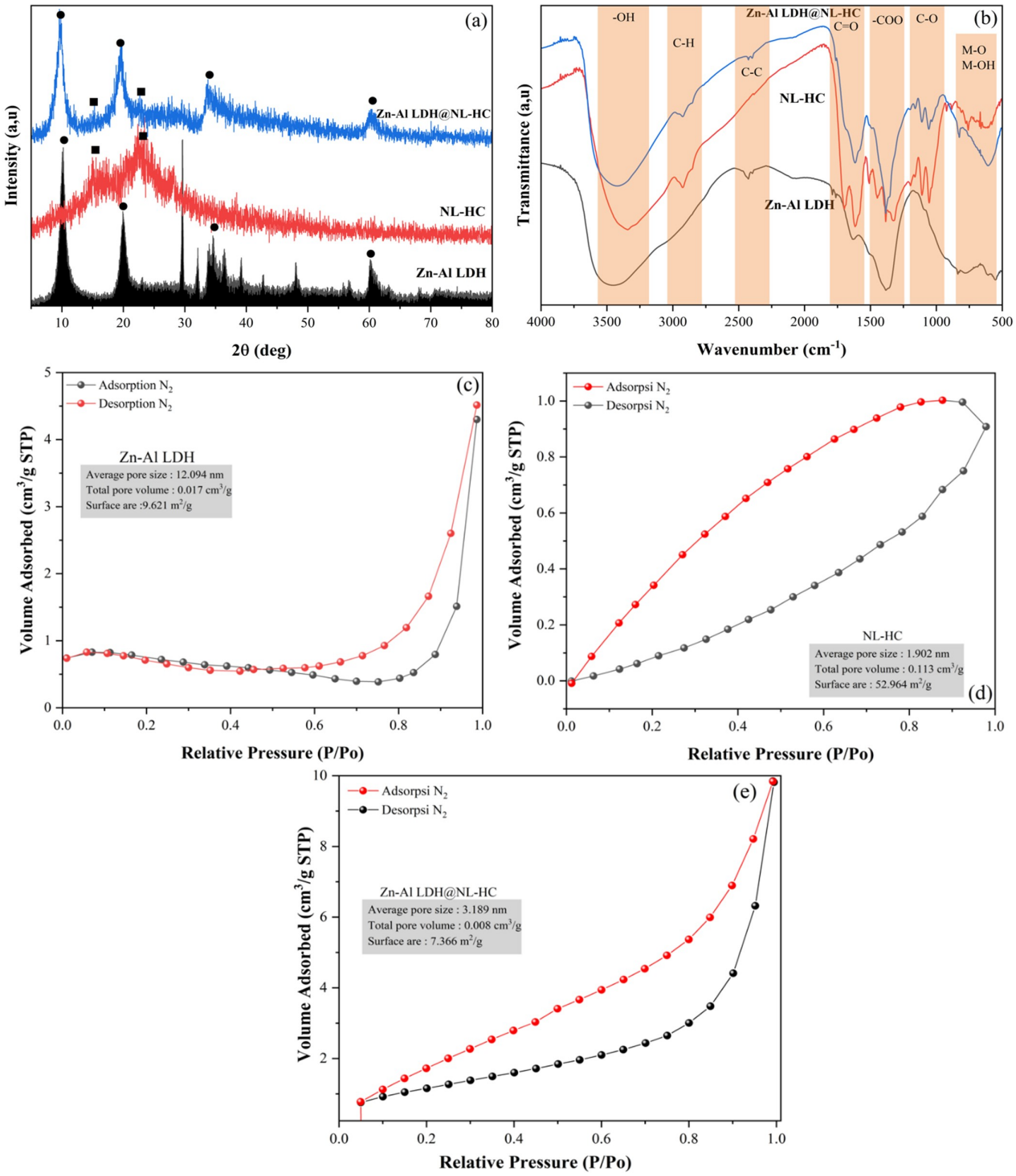

Figure 1. (a) XRD Patterns, (b) FT-IR Spectra, and (c-e) N_2 Adsorption-Desorption Isotherms of Zn-Al LDH, NL-HC, and Zn-Al LDH@NL-HC Composites

characteristics. Once the hydrochar is integrated with the Zn-Al LDH, the spherical hydrochar adheres to the Zn-Al LDH surface. In addition, there is a reduction in plate accumulation on the surface of Zn-Al LDH. The particle size varies with a dominance of 0.004 μm in Zn-Al LDH@NL-HC due to the interaction between Zn-Al and hydrochar from rambutan peel. In addition, hydrothermal carbonization treatment causes particle deaggregation resulting in varying particle sizes in Zn-Al

LDH@NL-HC (Fitri and Ardiansyah, 2023; Lin et al., 2023). Data on the percentage composition of Zn-Al LDH@NL-HC materials is shown in Table 1. The increase in the composition of O in Zn-Al LDH@NL-HC due to the oxygen function group in hydrochar successfully enriched the active site of Zn-Al LDH. The phenomenon verifies the formation of Zn-Al LDH@NL-HC adsorbent material.

Table 1. Composition of the Material Based on EDX Results

Element (%wt)	Material	
	ZnAl LDH	Zn-Al LDH@NL-HC
Zn	48.3	32.9
Al	4.9	6.8
O	38.2	46.5
Na	6.4	10
Si	2.2	-
N	-	3.8

TGA-DTA analysis aims to evaluate thermal stability, mass change, and thermal events in materials. The initial stage of Zn-Al LDH decomposition occurs at 100°C as shown in Figure 3. The endothermic peak indicates the loss of water molecules that are absorbed by fissorption and intercalation in Zn-Al LDH (Harb et al., 2025). The same phenomenon also occurs in Zn-Al LDH@NL-HC which can confirm the layered structure of LDH. The second stage of decomposition is characterized by the loss of volatile compounds at a temperature of 400°C. The dehydration of the brucite layer and the decomposition of nitrate ions that occupy the space between the layers are the beginning of the start of the second stage. Exothermic peaks in NL-HC appear between 320°C and 420°C associated with low-stability functional group decomposition. In Zn-Al LDH and Zn-Al LDH@NL-HC, LDH decomposition occurs into oxides and collapse of the layered structure. The third stages occur at temperatures of 450-800°C. The decomposition of carbon compounds in Zn-Al LDH@NL-HC composite materials also occurs in these two stages which is caused by the breakdown of cellulose, hemicellulose, lignin, and labile organic structures (Zhang et al., 2026). These findings highlight the stability of the LDH structure and the rearrangement of the carbon matrix in regulating the stability of high temperatures in the hydrothermal carbonization process.

3.2 Adsorption Performance and Fe(II) Removal Mechanism Analysis

3.2.1 Impact of pH

The dissociation equilibrium and chemical behavior of Fe(II) ions in the solution are affected by the acidity or alkaline conditions of the reaction medium. pH variation is a crucial parameter that controls the chemical specification of Fe(II) in the solution as well as the surface charge of the adsorbent, thus directly affecting the adsorption capacity. Based on Figure 4a, the Adsorption capacity of Fe(II) by Zn-Al LDH@NL-HC increases sharply from the very acidic condition to the maximum at pH 6. Meanwhile, the adsorption capacity of NL-HC is the lowest compared to the other two materials in Fe(II) adsorption. The adsorption capacity of Zn-Al LDH@NL-HC is higher than that of Zn-Al LDH because NL-HC can enrich the active sites of the composite through oxygen function groups. The findings suggest that the interaction between Fe^{2+} ions and the active site of the adsorbent becomes most effective under near-neutral conditions.

The high concentration of H^+ ions at low pH leads to strong competition with Fe^{2+} to occupy the negatively charged active group and causes the protonation of the adsorbent surface which decreases the adsorption activity of Zn-Al LDH@NL-HC (Elsheref et al., 2024). However, as the pH increases towards 6, there is deprotonation of the hydroxyl function group and surface oxygen. The phenomenon generates a greater negative charge and increases affinity to Fe^{2+} through electrostatic interactions and surface complexation. In addition, at this pH Fe(II) is still dominant as a stable Fe^{2+} dissolved species, so that the adsorption process takes place optimally without precipitation disturbances. When pH exceeds 6, the adsorption capacity decreases gradually as hydroxy species such as $Fe(OH)^+$ and $Fe(OH)_2$ begin to form which tend to settle as $Fe(OH)_2$ solids (Khandamov et al., 2025; Mangayarkarasi et al., 2023). The formation of such precipitates reduces the number of free Fe^{2+} ions available for adsorption and can mask or block pores and adsorbent active sites. Therefore, pH 6 is selected as the pH of the solution for other parameter tests.

3.2.2 Evaluation of Kinetics, Isotherm Models, and Thermodynamic Properties

The adsorption kinetics model can evaluate the adsorbent rate of Fe^{2+} ions adsorbent and understand the mechanisms that control the adsorption process over time. The adsorption kinetics of Fe(II) in Zn-Al LDH, NL-HC, Zn-Al LDH@NL-HC show a rapid increase in adsorption capacity in the early stages, then slow down to reach equilibrium at 120 min (Figure 4b). This indicates the gradual saturation of the active site of the adsorbent that has been fully filled with Fe(II) ions (Eletta et al., 2023). In the initial phase, the high adsorption rate is due to the abundance of available active sites and the large concentration gradient between the solution and the adsorbent surface. Zn-Al LDH@NL-HC composite (51.501 $mg.g^{-1}$) exhibits a much higher adsorption capacity than Zn-Al LDH (15.692 $mg.g^{-1}$) and NL-HC (8.594 $mg.g^{-1}$). The phenomenon indicates a synergistic effect between the LDH layered structure and the hydrochar porous carbon matrix (Ahmad et al., 2022). The presence of NL-HC increases the specific surface area, pore volume, and number of functional groups of oxygen, thus providing more binding sites for Fe^{2+} ions. This has been verified by BET and FTIR. Table 2 shows that the modeling of adsorption kinetics in Zn-Al LDH@NL-HC, NL-HC, and Zn-Al LDH composites is more in line with the PSO model in terms of R^2 values. In PSO, there is involvement of stronger chemical interactions such as ion exchange or surface com-

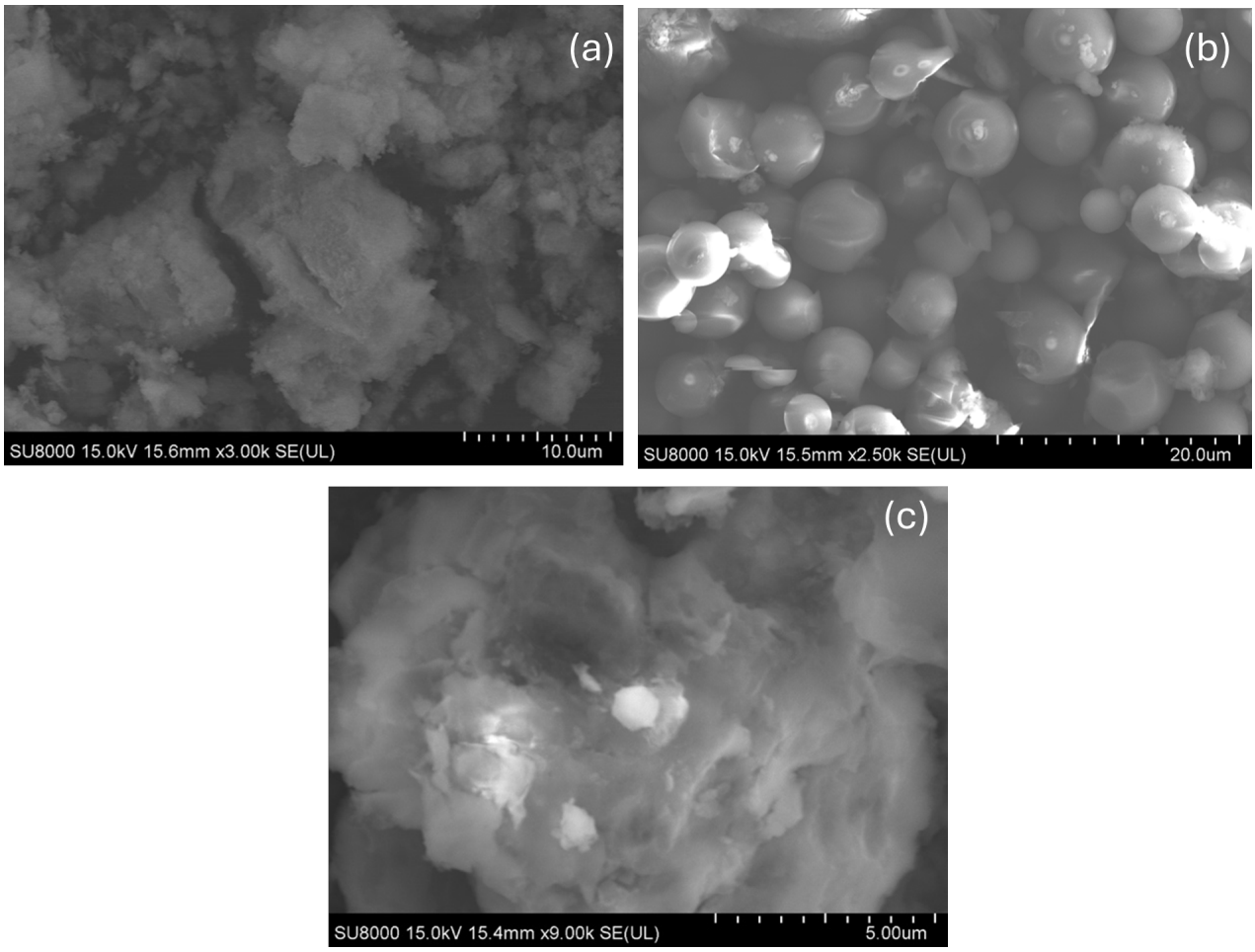

Figure 2. SEM Images of (a) Zn-Al LDH, (b) NL-HC, and (c) Zn-Al LDH@NL-HC Composites

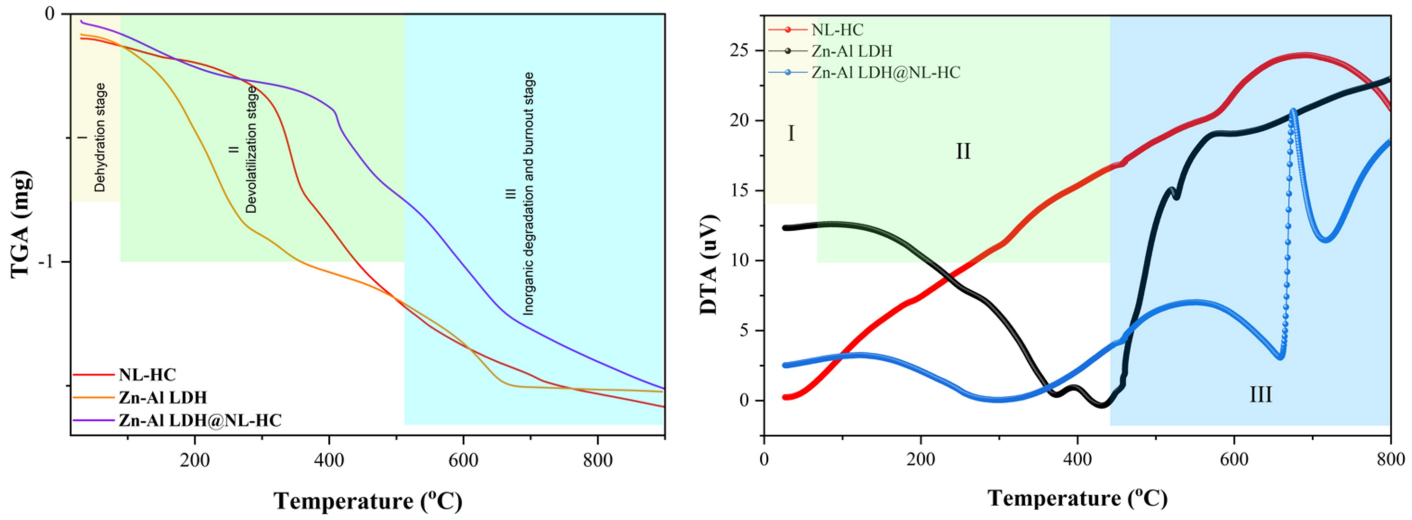

Figure 3. TGA-DTA Curves of Zn-Al LDH, NL-HC, and Zn-Al LDH@NL-HC Composites

plexation on the Fe(II) adsorption mechanism (Amri et al., 2024; Ramadhan et al., 2025). Overall, these results show that Zn-Al LDH@NL-HC composites are not only more efficient at adsorbing Fe(II) but also have faster and more practical

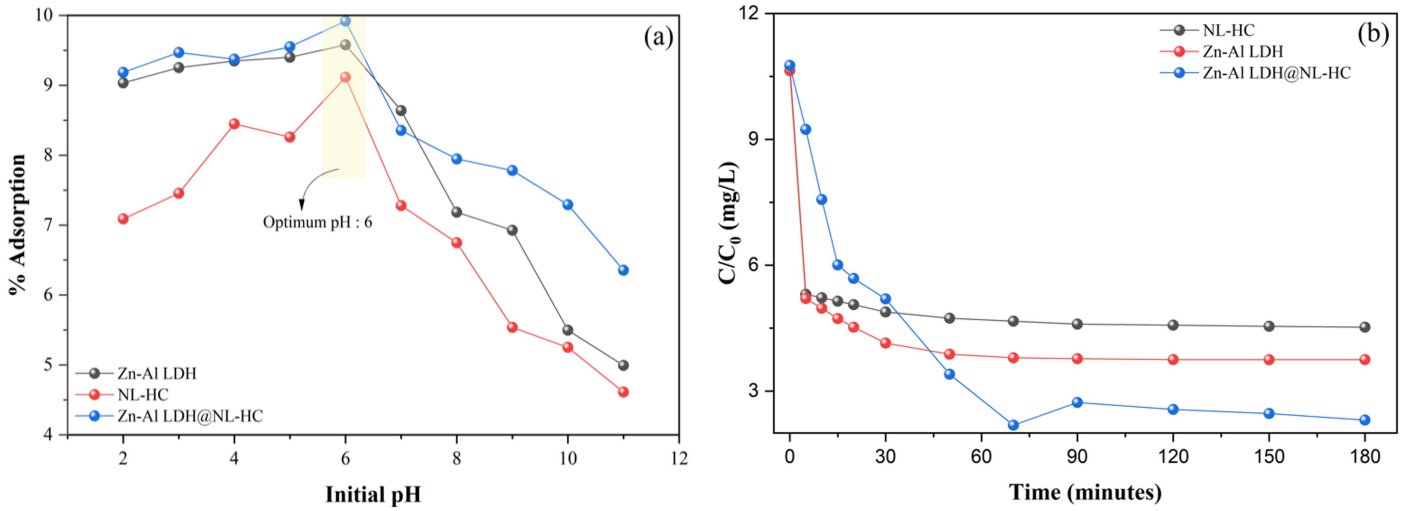

Figure 4. Effect of (a) pH Variation and (b) Adsorption Kinetics of Zn-Al LDH, NL-HC, and Zn-Al LDH@NL-HC Composites

adsorption dynamics for water treatment applications.

The analysis of Fe(II) adsorption isotherms aims to understand the relationship between the number of Fe^{2+} ions adsorbed on the adsorbent surface and the concentration of Fe(II) remaining in the solution under equilibrium conditions. Zn-Al LDH and Zn-Al LDH@NL-HC have an increased adsorption capacity as the temperature rises from 30 to 60 °C as shown in Table 3. Based on the Langmuir model, the Q_{max} value of Zn-Al LDH@NL-HC (76.336 $mg.g^{-1}$) was consistently higher than NL-HC (41.494 $mg.g^{-1}$) and Zn-Al LDH (25.126 $mg.g^{-1}$) at 60°C, the value of the Langmuir constant (K_L) that increases with temperature indicates that the affinity of the adsorbent to Fe(II) is also getting stronger under higher thermal conditions (Ahmad et al., 2024; Wijaya et al., 2025). Meanwhile, the Freundlich parameter shows a value of $n > 1$ for all conditions, which indicates adsorption takes place favorably on heterogeneous surfaces through multilayer interactions (Mandale et al., 2024). A comparison of the coefficient of determination (R^2) indicates that the Langmuir model generally provides a better match for both materials. The Langmuir model also indicates a strong affinity between the Fe^{2+} and the active site which is often associated with specific chemical interactions or surface bonds. The findings imply that Fe(II) adsorption tends to be dominated by the formation of monolayer layers at homogeneous sites.

All samples had a positive enthalpy change value (ΔH) at various initial concentrations as shown in Table 4. The findings confirm that the adsorption process is endothermic and more advantageous at higher temperatures. The ΔH value of the Zn-Al LDH@NL-HC composite is generally greater than that of Zn-Al LDH and NL-HC which implies a higher energy requirement to activate the adsorption site (Badaruddin et al., 2026). Positive entropy changes (ΔS) for both materials showed increased irregularities at the solid-solution interface of Fe^{2+} ions during the adsorption process. This occurs due to the release of hydrated water molecules from the surface of the adsorbent and Fe^{2+} ions. A negative Gibbs free energy value (ΔG) under most temperature conditions indicates that adsorption takes place spontaneously (El Jery et al., 2024). Zn-Al LDH@NL-HC composites consistently exhibit more negative ΔG values than Zn-Al LDH, thus creating a higher spontaneity of Fe(II) adsorption. Therefore, these results confirm that Zn-Al LDH@NL-HC has superior adsorption performance over pure ZnAl LDH in terms of interaction strength and process spontaneity.

3.2.3 Desorption and Reusability Studies

The desorption experiment aims to evaluate the ability of Fe^{2+} ions to be re-released from the adsorbent surface after the adsorption process has taken place. Figure 5a shows that desorption using the HNO_3 reagent is best suited for the Fe(II) metal ion desorption process. The desorption ability can reach 70.82%, 52.95%, and 31.54% for Zn-Al LDH, NL-HC, Zn-Al LDH@NL-HC respectively. This phenomenon is related to the property of HNO_3 as a strong acid that is perfectly dissociated in the solution producing H^+ and NO_3^- ions thus increasing the concentration of protons around the adsorbent surface (Tesi et al., 2025). This will encourage ion exchange and the active site on the adsorbent will be protonated so that it can weaken the interaction of metal ions. In addition, the H^+ ions will replace the Fe^{2+} ions that are bound to the adsorbent surface. This process shows that Fe(II) desorption does not only involve physical release but is dominated by chemical interactions in the form of ion exchange and surface bond breaking (Alhattab et al., 2023). Therefore, HNO_3 eluents achieve the highest percentage of desorption so they are best suited for desorption processes.

The regeneration test is carried out to determine the adsorbent ability after repeated use so that the structural stability of the material can be evaluated. Zn-Al LDH@NL-HC exhibits

Table 2. Kinetic Parameters for Fe(II) Adsorption onto Zn-Al LDH, NL-HC, and Zn-Al LDH@NL-HC

Adsorbent	Q_{exp} (mg/g)	Pseudo First Order			Pseudo Second Order		
		Q_{cal} (mg/g)	R^2	k_1	Q_{cal} (mg/g)	R^2	k_2
Zn-Al LDH	15.692	19.094	0.994	0.052	16.611	0.998	0.007
NL-HC	8.594	8.390	0.992	0.024	12.115	0.998	0.001
Zn/Al LDH@NL-HC	51.501	42.227	0.966	0.042	58.824	0.986	0.0008

Table 3. Isotherm Parameters for Fe(II) Adsorption onto Zn-Al LDH, NL-HC, and Zn-Al LDH@NL-HC

Adsorbent	Temp (°C)	Adsorption Isotherm Model					
		Langmuir			Freundlich		
		Q_m	K_L	R^2	n	K_F	R^2
Zn-Al LDH	30	20.040	0.161	0.898	1.745	2.616	0.822
	40	24.510	0.115	0.969	2.053	3.963	0.866
	50	25.063	0.171	0.978	2.293	5.349	0.846
	60	25.126	0.319	0.996	2.918	8.032	0.867
NL-HC	30	34.247	0.126	0.892	1.914	5.482	0.712
	40	37.175	0.140	0.921	1.932	6.307	0.750
	50	37.313	0.224	0.969	2.189	8.698	0.786
	60	41.494	0.192	0.881	2.262	9.605	0.613
Zn/Al LDH@NL-HC	30	54.348	0.107	0.739	1.527	6.350	0.701
	40	56.180	0.151	0.754	1.649	8.794	0.708
	50	58.480	0.209	0.934	1.663	10.889	0.876
	60	76.336	0.289	0.575	1.607	17.968	0.619

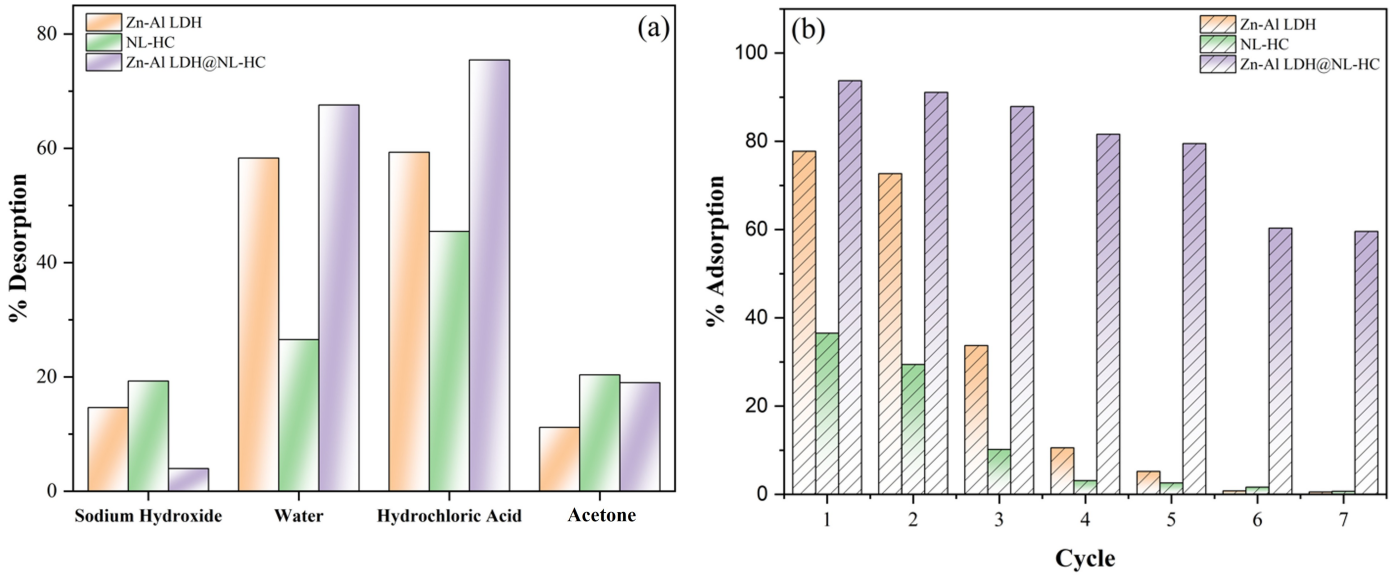

Figure 5. (a) Desorption Efficiency and (b) Regeneration Performance of Zn-Al LDH, NL-HC, and Zn-Al LDH@NL-HC

a more stable structure than Zn-Al LDH (Figure 5b). The adsorption activity of the composite material only decreased by 5.85% from 93.73% to 87.88% until the third cycle. Meanwhile, the adsorption performance of ZnAl LDH and NL-HC were only at 5.21% and 2.58% after cycle five. When cycle five is reached, Zn-Al LDH@NL-HC can still maintain structural

Table 4. Thermodynamic Parameters for Fe(II) Adsorption onto Zn-Al LDH, NL-HC, and Zn-Al LDH@NL-HC

C_0 mg/L	T (°C)	ΔH (kJ/mol)			ΔS (J/mol.K)			ΔG (kJ/mol)		
		Zn-Al	NL-HC	Composite	Zn-Al	NL-HC	Composite	Zn-Al	NL-HC	Composite
10	30	16.807	37.281	31.158	0.062	0.123	0.111	-2.010	0.063	-2.586
	40							-2.632	-1.165	-3.699
	50							-3.253	-2.394	-4.813
	60							-3.874	-3.622	-5.927
20	30	28.749	26.321	41.227	0.103	0.087	0.147	-2.337	-0.120	-3.455
	40							-3.363	-0.992	-4.929
	50							-4.389	-1.865	-6.404
	60							-5.415	-2.738	-7.879
30	30	18.041	20.052	28.766	0.068	0.066	0.108	-2.596	-0.008	-3.925
	40							-3.277	-0.670	-5.004
	50							-3.958	-1.332	-6.083
	60							-4.639	-1.994	-7.162
40	30	14.751	15.478	48.037	0.052	0.048	0.167	-0.985	0.939	-2.656
	40							-1.504	0.460	-4.329
	50							-2.023	-0.020	-6.002
	60							-2.543	-0.500	-7.675
50	30	15.895	13.114	39.417	0.052	0.037	0.134	0.069	1.824	-1.300
	40							-0.454	1.452	-2.644
	50							-0.976	1.079	-3.988
	60							-1.498	0.706	-5.332

Table 5. Several Studies Reported in the Literature have Investigated Fe(II) Adsorption

Adsorbent	Adsorption Parameters				Q_{max} (mg.g^{-1})	Ref
	pH	Equilibrium time (min)	Dosage (g.L^{-1})	Temperature (K)		
Prunus armeniaca stone	7	120	-	298	42.0	(Elsheref et al., 2024)
Modified bentonite	5.2	40	1	308	10.84	(Khandamov et al., 2025)
Lagenaria siceraria Stem	6.5	30	0.5	333	78.09	(Mangayarkarasi et al., 2023)
Theobroma cacao/activated carbon	-	120	4	303	37.45	(Eletta et al., 2023)
Sodium alginate-Poly(acrylonitrile-co-styrene)/CNTs	3	80	1.6	-	85	(Mohamed et al., 2024)
Chitosan/activated carbon	6	80	30	45	0.347	(Wulan et al., 2022)
Activated Carbon from Balanites Aegyptiaca Seed Shells	-	5	0.2	298	126.35	(Kada et al., 2024)
NiAl LDH/Biochar	-	-	-	303	104.167	(Palapa et al., 2023b)
NL-HC	6	120	1	333	41.494	This study
Zn-Al LDH	6	120	1	333	25.126	
Zn-Al LDH@NL-HC	6	120	1	333	76.336	

stability by having an adsorption activity of 79.48%. This high stability can be explained by the role of NL-HC as a porous carbon matrix that functions as a structural buffer on LDH sheets. In addition, organic components of hydrochars such as the –OH group of cellulose can form additional bonds with LDH thereby strengthening the integrity of the composite (Palapa et al., 2023a). Therefore, the incorporation of hydrochar not only increases the adsorption capacity, but also significantly increases the structural resistance of the material making it economically advantageous. This is confirmed by Table 5 which shows a comparison of the adsorption capacity and parameters in this study with previous studies on degrading Fe(II).

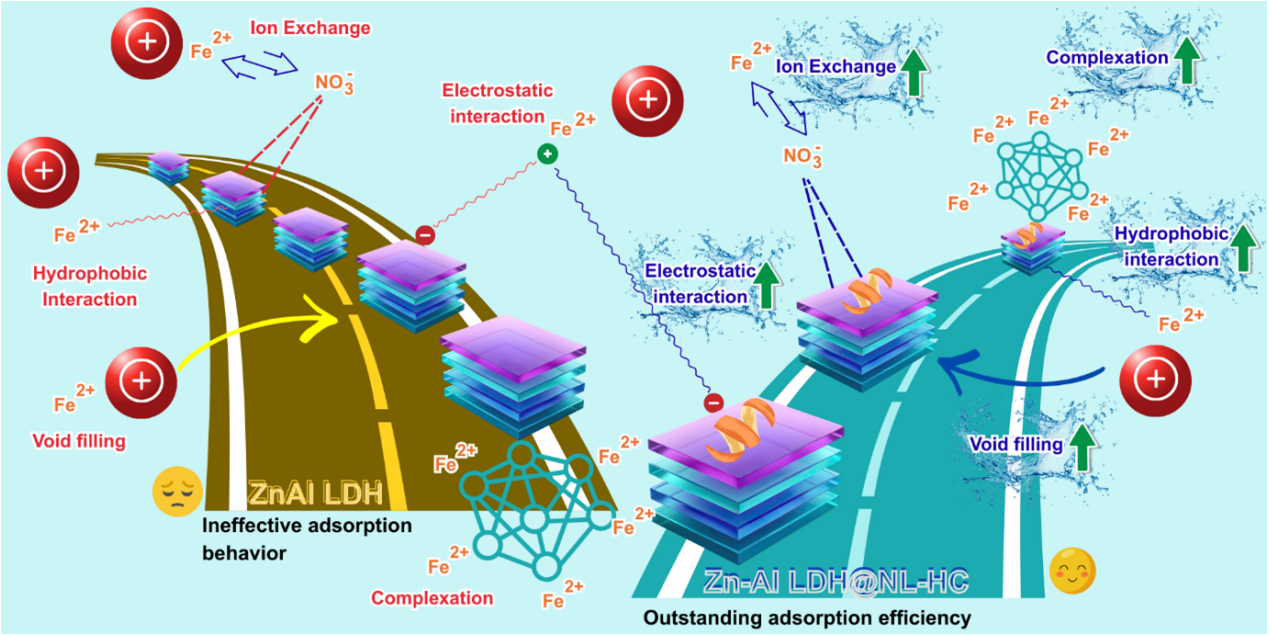

Figure 6. The Possible Mechanism of Fe(II) Adsorption Enhancement

3.2.4 Proposed Mechanism for NOR Adsorption

The adsorption mechanism of Fe(II) by Zn-Al LDH@NL-HC composite illustrated in Figure 6 involves several synergistic interactions between the layered structure of LDH and the hydrocarbon matrix rich in oxygen groups. Fe^{2+} ions can be adsorbed through the pores of Zn-Al LDH@NL-HC by a diffusion approach from the solution to the adsorbent surface. In addition, the negative surface charge that increases at pH close to neutral due to the deprotonation of hydroxyl groups and oxygen allows for the occurrence of strong electrostatic attraction to the Fe^{2+} cation (Fitri and Ardiansyah, 2023). Furthermore, Fe^{2+} can bind through a surface complexation mechanism with oxygen-rich groups such as, –OH in hydrochar. In addition, the exchange of Fe^{2+} ions with interlayer anions or metal sites on LDH structures can also occur. The dominant Langmuir isothermal model shows that adsorption mainly takes place as the formation of a monolayer at a relatively homogeneous active site with a high affinity to Fe^{2+}. PSO model in Zn-Al LDH@NL-HC indicates the involvement of chemical attractions such as ion exchange or surface complexation. Therefore, the increased performance of Zn-Al LDH@NL-HC compared to Zn-Al LDH is associated with synergistic effects in the form of the addition of oxygen-based active sites and higher porosity. In addition, the combination of electrostatic, complexation, and ion exchange mechanisms can effectively bind Fe(II).

4. CONCLUSIONS

In this study, a Zn-Al LDH modified with rambutan-peel hydrochar was successfully synthesized (Zn-Al LDH@NL-HC) and demonstrated markedly enhanced performance for Fe(II) removal from aqueous solutions compared with the individual components. Comprehensive physicochemical characterization confirmed that hydrochar incorporation improved surface area, pore structure, oxygen-containing functional groups, and structural stability, thereby creating abundant active sites for metal adsorption. Adsorption behavior was strongly influenced by solution pH, with near-neutral conditions promoting electrostatic attraction and surface complexation while minimizing competition from protons and metal precipitation. Kinetic, isotherm, and thermodynamic analyses collectively indicated that the adsorption process was rapid, favorable, spontaneous, and endothermic, proceeding predominantly through monolayer formation on energetically favorable sites. The superior performance of the composite was attributed to synergistic mechanisms involving diffusion into mesopores, electrostatic interactions, surface complexation with oxygen-rich groups, and ion exchange within LDH. Furthermore, regeneration studies revealed that the composite maintained high structural integrity and adsorption efficiency over repeated cycles, highlighting its strong potential as a sustainable and efficient adsorbent for heavy metal remediation in water treatment applications.

5. ACKNOWLEDGEMENT

This study received financial and institutional support from the Research Center of Inorganic Materials and Coordination Complexes, Universitas Sriwijaya. The authors would also like to express their sincere gratitude to Prof. Aldes Lesbani, Ph.D for his valuable suggestions and insightful advice that greatly contributed to the improvement and refinement of this paper.

REFERENCES

Ahmad, N., Rohmatullaili, A. Wijaya, and A. Lesbani (2024). Magnetite Humic Acid-Decorated MgAl Layered Double Hydroxide and Its Application in Procion Red Adsorption. *Colloids and Surfaces A: Physicochemical and Engineering Aspects*, **684**; 133042

Ahmad, N., F. Suryani, I. Royani, and A. Lesbani (2022). Adsorption of Methylene Blue on Magnetite Humic Acid: Kinetic, Isotherm, Thermodynamic, and Regeneration Studies. *Results in Chemistry*, **4**; 100629

Alcalde-Garcia, F., S. Prasher, S. Kaliaguine, J. R. Tavares, and M.-J. Dumont (2023). Desorption Strategies and Reusability of Biopolymeric Adsorbents and Semisynthetic Derivatives in Hydrogel and Hydrogel Composites Used in Adsorption Processes. *ACS Engineering Au*, **3**(6); 443–460

Alhattab, Z. D., A. M. Aljeboree, M. A. Jawad, F. S. Sheri, A. K. O. Aldulaim, and A. F. Alkaim (2023). Highly Adsorption of Alginate/bentonite Impregnated TiO_2 Beads for Wastewater Treatment: Optimization, Kinetics, and Regeneration Studies. *Caspian Journal of Environmental Sciences*, **21**(3); 657–664

Amri, A., S. Wibiyan, A. Wijaya, N. Ahmad, R. Mohadi, and A. Lesbani (2024). Efficient Adsorption of Methylene Blue Dye Using Ni/Al Layered Double Hydroxide-Graphene Oxide Composite. *Bulletin of Chemical Reaction Engineering & Catalysis*, **19**(2); 181–189

Asri, F., N. Palapa, T. Taher, A. Rachmat, and A. Lesbani (2020). Efficient Removal of Methylene Blue by Adsorption Using Composite Based Ca/Al Layered Double Hydroxide-Biochar. *Global NEST Journal*, **22**(2); 250–257

Badaruddin, M., L. Hanum, E. Melwita, S. Wibiyan, Y. Hanifah, and A. Lesbani (2026). Temperature-Tailored Cellulose-Rich *Cladophora Sp*. Hydrochar for Selective Malachite Green Adsorption from Multi-Dye Systems. *Biochemical Engineering Journal*, **226**; 109986

Bai, Y., R. Ma, Z. Jing, X. Wan, J. Tong, W. Huang, and J. Liu (2024). Synthesis of Zn/Al Layered Double Hydroxides Magnetic-nanoparticle for Removal of Humic Acid. *Desalination and Water Treatment*, **317**; 100097

Cedeño-Muñoz, J. S., B. J. Zumarraga-Valencia, J. E. Cevallos-Mendoza, B. F. Rivadeneira-Mendoza, I. B. Pérez-Almeida, K. K. Yadav, M. D. Saquete, N. Boluda-Botella, and J. M. Rodríguez-Díaz (2026). Hydrochar-Based Mg-Fe Layered Double Hydroxide Hybrid for Efficiency Removal of Tetracyclines from Water and Reuse Across Multiple Cycles. *Emerging Contaminants*, **12**(1); 100623

Durak, H., R. Z. Yarbay, and B. Atilgan Türkmen (2026). Hydrothermal Carbonization of Biomass for Hydrochar Production: Mechanisms, Process Parameters, and Sustainable Valorization. *Processes*, **14**(2); 339

El Jery, A., H. S. K. Alawamleh, M. H. Sami, H. A. Abbas, S. S. Sammen, A. Ahsan, M. Imteaz, A. Shanableh, M. Shafiquzzaman, and H. Osman (2024). Isotherms, Kinetics and Thermodynamic Mechanism of Methylene Blue Dye Adsorption on Synthesized Activated Carbon. *Scientific Reports*, **14**(1); 970

El-Sawaf, A. K., A. A. Nassar, A. Ebada, and M. F. Mubarak (2025). Chemically Activated Biochar Layered Double Hydroxide Composites for Multifunctional Water Remediation: Coupled Adsorption, Ion Exchange, and Catalytic Degradation Mechanisms. *Inorganic Chemistry Communications*, **184**; 115977

Eletta, O. A., F. O. Ayandele, and J. O. Ighalo (2023). Adsorption of Pb(II) and Fe(II) by Mesoporous Composite Activated Carbon from *Tithonia diversifolia* Stalk and *Theobroma Cacao* Pod. *Biomass Conversion and Biorefinery*, **13**(11); 9831–9840

Elsheref, M., A. Ahmed, E. Elmelegy, M. A. Tarr, W. Hammad, and M. Darweesh (2024). Adsorptive Potential of Apricot (*Prunus Armeniaca*) Stone in the Removal of Cr(VI) and Fe(II) Ions from Aquatic Systems: Kinetic and Isothermal Investigations. *Journal of Hazardous Materials Advances*, **16**; 100498

Fitri, E. S. and R. Ardiansyah (2023). Study and Characterization of Hydrochar from Duku (*Lansium domesticum*) Peel. *Indonesian Journal of Material Research*, **1**(2); 44–50

Gao, D., W. Zhang, H. Dong, Y. Yu, W. Liu, H. Luo, Z. Jing, B. Liang, L. Peng, B. Wu, et al. (2025). Phosphorus Removal from Water by the Layered Double Hydroxides (LDHs)-Based Adsorbents: A Review for Structure, Mechanism, and Current Progress. *Environmental Technology & Innovation*, **37**; 104003

Hadnadjev-Kostic, M., T. Vulic, D. Karanovic, A. Tomic, and D. Cvetkovic (2025). Layered Double Hydroxide-Based Materials for Wastewater Treatment: Recent Progress in Multifunctional Environmental Applications. *Processes*, **13**(12); 3757

Hamad, N., A. A. Galhoum, A. Saad, and S. Wageh (2024). Efficient Adsorption of Cationic and Anionic Dyes Using Hydrochar Nanoparticles Prepared from Orange Peel. *Journal of Molecular Liquids*, **409**; 125349

Hao, H. (2025). Engineered LDH-Alginate Composite Hydrogel Columns for Selective Heavy Metal Removal. *Frontiers in Chemistry*, **13**; 1649831

Harb, A. H., A. M. Elewa, R. R. Sheha, H. H. Someda, and M. R. Mahmoud (2025). Efficient Adsorption of $^{152+154}$Eu(III) by Surfactant Modified Mg/Al Layered Double Hydroxide. *Applied Radiation and Isotopes*, **225**; 112054

Huang, Y., C. Liu, S. Rad, H. He, and L. Qin (2022). A Comprehensive Review of Layered Double Hydroxide-Based Carbon Composites As an Environmental Multifunctional Material for Wastewater Treatment. *Processes*, **10**(4); 617

Jefri, J., N. A. Fithri, F. S. Arsyad, M. Mardiyanto, Y. Hanifa, and A. Lesbani (2025). Boosting Photocatalytic Efficiency: LDH Modified with Gambier Leaf Extract for Tetracycline Degradation. *Next Materials*, **7**; 100633

Juleanti, N., N. R. Palapa, T. Taher, N. Hidayati, B. I. Putri, and A. Lesbani (2021). The Capability of Biochar-Based CaAl and MgAl Composite Materials as Adsorbent for Re-

moval Cr(VI) in Aqueous Solution. *Science and Technology Indonesia*, **6**(3); 196–203

Kada, D., D. Domga, C. Asobo, N. Taybe, and J. Kowe (2024). Adsorption of Iron (II) from Aqueous Solution by Activated Carbon from Desert Date Seed Shells (Balanites Aegyptiaca). *World Journal of Applied Chemistry*, **9**(3); 44–55

Khan, S., S. Ajmal, T. Hussain, and M. U. Rahman (2025). Clay-Based Materials for Enhanced Water Treatment: Adsorption Mechanisms, Challenges, and Future Directions. *Journal of Umm Al-Qura University for Applied Sciences*, **11**(2); 219–234

Khandamov, D. A., T. A. Kurniawan, A. S. Bekmirzayev, F. Batool, D. Khandamova, S. Nurullayev, S. Kholikova, Z. Babakhanova, and M. M. Hayet Khan (2025). Enhanced Adsorption of Fe(II) from Synthetic Wastewater Using Modified Bentonite: Isotherms, Kinetics, Thermodynamics, and Adsorption Mechanisms. *Microporous and Mesoporous Materials*, **384**; 113451

Khir, N. H. M., N. F. Muhamad Salleh, N. Abdul Ghafar, N. Mohd Shukri, and R. Jusoh (2025). Preparation and Characterization of Modified Rambutan Peels for the Removal of Chromium(VI) and Nickel(II) from Aqueous Solution: Environmental Impact and Optimization. *Malaysian Journal of Analytical Sciences*, **29**(1); 1292

Khosrowshahi, M. S., M. A. Abdol, H. Mashhadimoslem, E. Khakpour, H. B. M. Emrooz, S. Sadeghzadeh, and A. Ghaemi (2022). The Role of Surface Chemistry on CO_2 Adsorption in Biomass-Derived Porous Carbons by Experimental Results and Molecular Dynamics Simulations. *Scientific Reports*, **12**(1); 8917

Kohzadi, S., N. Marzban, J. A. Libra, M. Bundschuh, and A. Maleki (2023). Removal of RhB from Water by Fe-Modified Hydrochar and Biochar – An Experimental Evaluation Supported by Genetic Programming. *Journal of Molecular Liquids*, **369**; 120971

Kudaibergenova, R. M., O. N. Nurlybayev, I. Kazarinov, A. N. Nurlybayeva, S. A. Orynbayev, N. S. Murzakasymova, E. A. Baibazarova, and A. A. Kabdushev (2026). Physicochemical Properties and Adsorption Mechanisms of Bentonite–Sawdust-Derived Carbon Composites. *Water*, **18**(2); 290

Kundu, S., T. Khandaker, M. A. A. M. Anik, M. K. Hasan, P. K. Dhar, S. K. Dutta, M. A. Latif, and M. S. Hossain (2024). A Comprehensive Review of Enhanced CO_2 Capture Using Activated Carbon Derived from Biomass Feedstock. *RSC Advances*, **14**(40); 29693–29736

Lesbani, A., N. Ahmad, S. Wibiyan, A. Wijaya, Amri, Y. Hanifah, I. Royani, and R. Mohadi (2025). Improving Congo Red Dye Removal by Modification Layered Double Hydroxide with Microalgae and Macroalgae: Characterization and Parametric Optimization. *Colloids and Surfaces A: Physicochemical and Engineering Aspects*, **706**; 135770

Lin, Z., R. Wang, S. Tan, K. Zhang, Q. Yin, Z. Zhao, and P. Gao (2023). Nitrogen-Doped Hydrochar Prepared by Biomass and Nitrogen-Containing Wastewater for Dye Adsorption: Effect of Nitrogen Source in Wastewater on the Adsorption Performance of Hydrochar. *Journal of Environmental Management*, **334**; 117503

Mandale, P., K. Kulkarni, K. Jadhav, A. Kulkarni, and R. Mahajan (2024). Adsorption of Malachite Green Dye from Aqueous Solution on Bioadsorbent as Low-Cost Adsorbent. *Materials Today: Proceedings*

Mangayarkarasi, A., S. Arivoli, and K. Veeravelan (2023). Fe(II) Ions' Adsorption Kinetics and Thermodynamics on Lagenaria Siceraria Stem Nano Carbon. *Ecology, Environment and Conservation*, **29**; 484–493

Meftah, S., K. Meftah, M. Drissi, I. Radah, K. Malous, A. Amahrous, A. Chahid, T. Tamri, A. Rayyad, B. Darkaoui, S. Hanine, O. El-Hassan, and L. Bouyazza (2025). Heavy Metal Polluted Water: Effects and Sustainable Treatment Solutions Using Bio-Adsorbents Aligned with the SDGs. *Discover Sustainability*, **6**(1); 137

Mohadi, R., N. Juleanti, N. R. Palapa, N. Hidayati, and A. Lesbani (2022). Development of Renewable Material Hydrochar-Based CaAl Layered Double Hydroxide to Overcome Methyl Red Dyes Contaminant. *Journal of Ecological Engineering*, **23**(3); 17–25

Mohamed, R., N. A. Al-Derbas, N. S. Al-Muaikel, M. A. Rafea, M. S. Alhumaimess, I. H. Alsohaimi, and H. M. Hassan (2024). Development and Characterization of Sodium Alginate Beads Incorporating Functionalized Poly (Acrylonitrile-Co-Styrene)/carbon Nanotubes for Effective Fe(II) Ion Adsorption from Aqueous Solutions. *International Journal of Biological Macromolecules*, **283**; 137947

Nassar, A. E., E. I. El-Aswar, S. A. Rizk, S. E. S. Gaber, and H. S. Jahin (2023). Microwave-Assisted Hydrothermal Preparation of Magnetic Hydrochar for the Removal of Organophosphorus Insecticides from Aqueous Solutions. *Separation and Purification Technology*, **306**; 122569

Normah, N. R. Palapa, T. Taher, R. Mohadi, H. P. Utami, and A. Lesbani (2021). The Ability of Composite Ni/Al-Carbon Based Material Toward Readsorption of Iron(II) in Aqueous Solution. *Science and Technology Indonesia*, **6**(3); 156–165

Palapa, N. R., N. Ahmad, H. P. Utami, Z. A. Zahara, R. Mohadi, and A. Lesbani (2023a). Adsorption of Phenol Using Hydrochar Modified Layered Double Hydroxide – Kinetic, Isotherm, and Regeneration Studies. *Ecological Engineering and Environmental Technology*, **24**(5); 275–281

Palapa, N. R., A. Wijaya, P. M. S. B. N. Siregar, A. Amri, N. Ahmad, T. Taher, and A. Lesbani (2023b). Adsorption of Fe(II) by Layered Double Hydroxide Composite with Carbon-Based Material (Biochar and Graphite): Reusability and Thermodynamic Properties. *Indonesian Journal of Chemistry*, **23**(1); 101–112

Ramadhan, N., M. Mardiyanto, N. A. Fithri, Y. Hanifah, and A. Lesbani (2025). Eco-Friendly Microwave-Assisted Synthesis of Ni/Al-Spirulina Platensis Hydrochar Composites for Efficient Ciprofloxacin Adsorption. *Sustainable Chemistry One World*, **8**; 100150

Ramadhan, N., M. Mardiyanto, N. A. Fitri, Y. Hanifah, and

A. Lesbani (2026). Selective Adsorption and Reusability of LDH@Microalgae (Spirulina) Hydrochar via Microwave-Assisted Synthesis for Ciprofloxacin Removal: Competitive Fluoroquinolone Adsorption and Mechanistic Insight. *Colloids and Surfaces A: Physicochemical and Engineering Aspects*, **739**; 140131

Shabbirahmed, A. M., A. Jacob, P. Dey, P. Somu, and D. Haldar (2025). Biomass as Eco-Friendly Adsorbents for the Removal of Emerging Pollutants from Wastewater: A Review. *Discover Applied Sciences*, **7**(7); 771

Shafie, M. E., M. F. Mubarak, M. Nasr, A. Shaltout, and A. El Shahawy (2025). Cobalt, Copper, and Manganese Contamination in Water: A Comprehensive Review. *Discover Water*, **1**(2); 65–79

Sikri, N., S. Kumar, B. Behera, and J. Mehta (2025). Graphene Oxide/Layered Double Hydroxide Composite as Highly Efficient and Recyclable Adsorbent for Removal of Ciprofloxacin from Aqueous Phase. *Frontiers in Nanotechnology*, **7**(2025); 1578620

Singh, V., G. Ahmed, S. Vedika, P. Kumar, S. K. Chaturvedi, S. N. Rai, E. Vamanu, and A. Kumar (2024). Toxic Heavy Metal Ions Contamination in Water and Their Sustainable Reduction by Eco-Friendly Methods: Isotherms, Thermodynamics and Kinetics Study. *Scientific Reports*, **14**(1); 7595

Taher, T., Y. G. Wibowo, S. Maulana, N. R. Palapa, A. Rianjanu, and A. Lesbani (2023). Facile Synthesis of Biochar/Layered Double Oxides Composite by One-Step Calcination for Enhanced Carbon Dioxide (CO_2) Adsorption. *Materials Letters*, **338**; 134068

Tee, G. T., X. Y. Gok, and W. F. Yong (2022). Adsorption of Pollutants in Wastewater via Biosorbents, Nanoparticles and Magnetic Biosorbents: A Review. *Environmental Research*, **212**; 113248

Tesi, G. O., O. Ejeromedoghene, Y. A. Alli, H. B. Okunoja, and A. R. Ipeaiyeda (2025). Adsorption and Desorption Performances of Eichhornia Crassipes (Water Hyacinth) Roots and Leaves Powder Toward Metal Ions in Industrial Wastewater. *Ovidius University Annals of Chemistry*, **36**(1); 1–12

Torgbo, S., P. Sukyai, U. Sukatta, S. Böhmdorfer, M. Beaumont, and T. Rosenau (2024). Cellulose Fibers and Ellagitannin-Rich Extractives from Rambutan (*Nephelium lappaceum* L.) Peel by an Eco-Friendly Approach. *International Journal of Biological Macromolecules*, **259**; 128857

Tyagi, U. and N. Anand (2024). Sustainable and Low-Cost Biomass Derived Adsorbents for the Removal of Toxic Contaminants from Wastewater: Approaches and Future Perspective. *Waste Management Bulletin*, **2**(2); 308–325

Wibiyan, S., I. Royani, N. Ahmad, and A. Lesbani (2024). Assessing the Efficiency, Selectivity, and Reusability of ZnAl-Layered Double Hydroxide and Eucheuma Cottonii Composite in Removing Anionic Dyes from Wastewater. *Inorganic Chemistry Communications*, **170**; 113347

Wijaya, A., N. Ahmad, L. Hanum, E. Melwita, Y. Hanifah, and A. Lesbani (2025). Biohybrid ZnCr-LDH/*Spirogyra Algae* Composite for Selective Adsorption from Multi-Dye Anionic Mixtures: Toward Enhanced Removal of Direct Yellow. *Next Materials*, **9**; 101094

Wijaya, A., P. M. S. B. N. Siregar, A. Priambodo, N. R. Palapa, T. Taher, and A. Lesbani (2021). Innovative Modified Cu-Al/C (C = Biochar, Graphite) Composites for Removal of Procion Red from Aqueous Solution. *Science and Technology Indonesia*, **6**(4); 228–234

Wulan, P., Y. Kusumastuti, and A. Prasetya (2022). Adsorption of Fe(II) Ion into Chitosan/Activated Carbon Composite: Isotherm and Kinetics Studies. *Journal of Engineering Science and Technology*, **17**(3); 2218–2233

Xiao, M., R. Hu, W. Gwenzi, R. Tao, X. Cui, H. Yang, and C. Noubactep (2024). Materials for Sustainable Metallic Iron-Based Water Filters: A Review. *Environmental Chemistry Letters*, **22**(4); 2113–2131

Yao, J., R. Yang, Y. Zhang, M. Zhu, M. Bi, K. Ma, Y. Liu, H. Xie, and Y. Wu (2025). Temporal and Spatial Distribution of Fe(II) and Dissolved Iron and Their Influencing Factors in the Yangtze River Estuary. *Continental Shelf Research*, **285**; 105385

Zhang, H., J. Sheng, C. Wang, and S. Yuan (2026). A New Application of Algae-Grass Biomass Within Watersheds: Employing Hydrochar to Control Dye Pollutant Emissions. *Journal of Cleaner Production*, **538**; 147286

